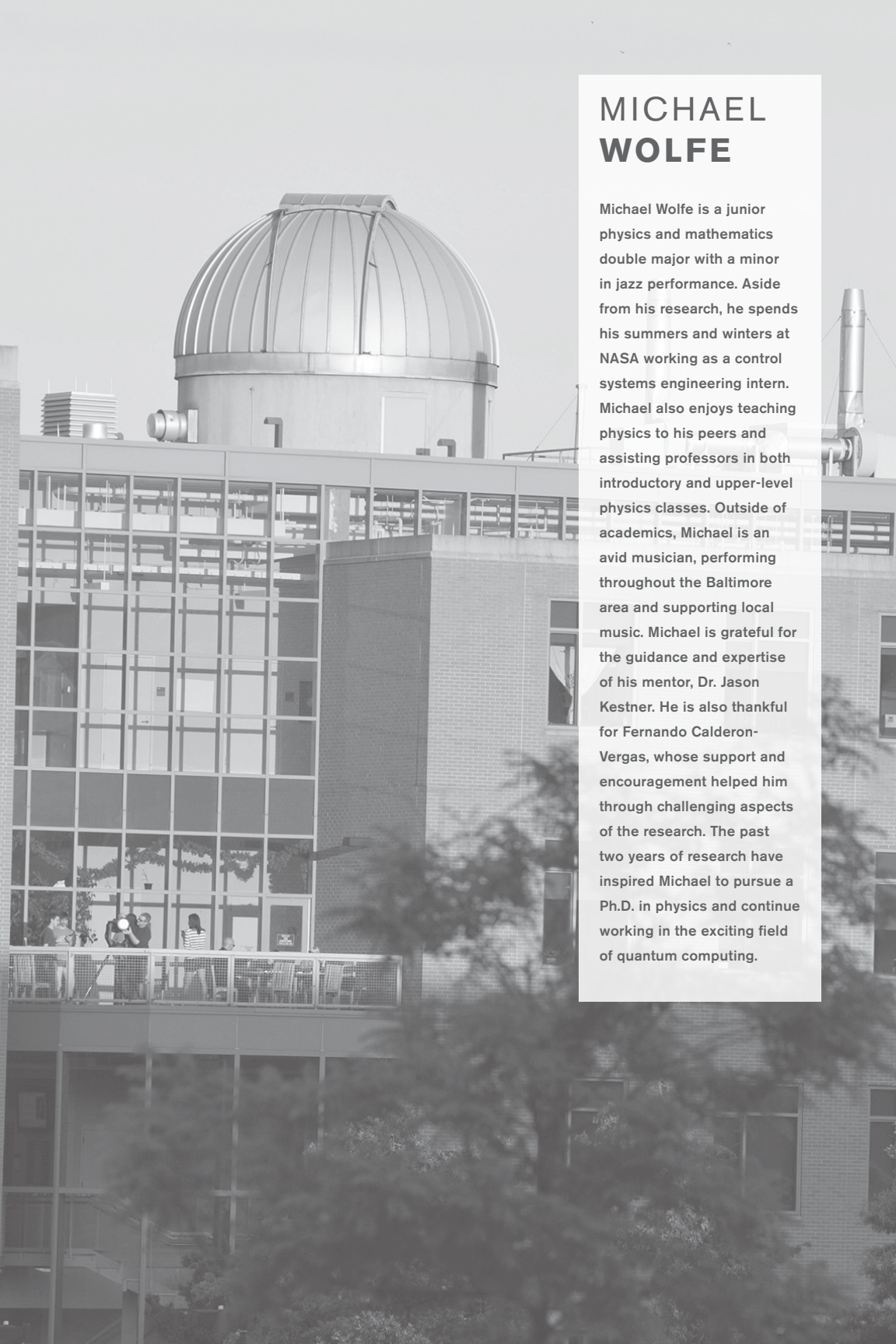

MICHAEL **WOLFE**

Michael Wolfe is a junior physics and mathematics double major with a minor in jazz performance. Aside from his research, he spends his summers and winters at NASA working as a control systems engineering intern. Michael also enjoys teaching physics to his peers and assisting professors in both introductory and upper-level physics classes. Outside of academics, Michael is an avid musician, performing throughout the Baltimore area and supporting local music. Michael is grateful for the guidance and expertise of his mentor, Dr. Jason Kestner. He is also thankful for Fernando Calderon-Vergas, whose support and encouragement helped him through challenging aspects of the research. The past two years of research have inspired Michael to pursue a Ph.D. in physics and continue working in the exciting field of quantum computing.

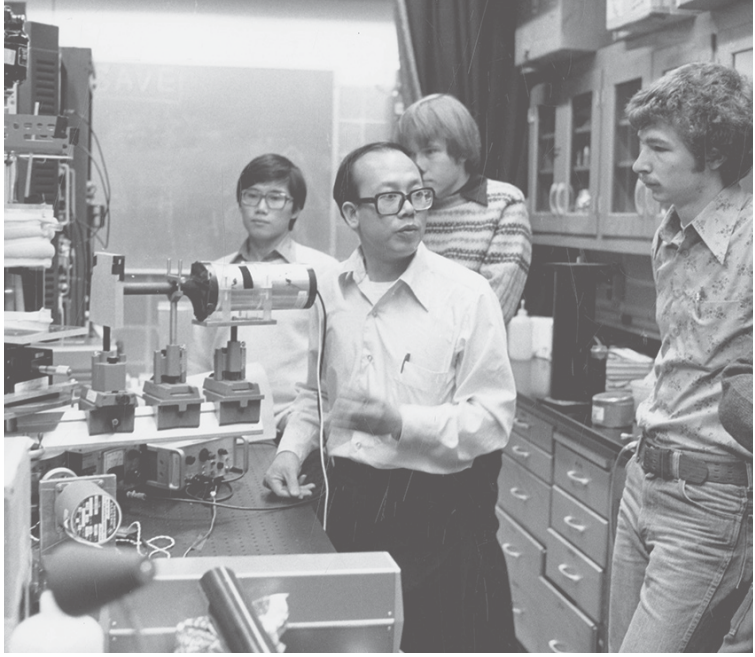

INCREASING THE SPEED OF QUANTUM LOGIC GATES IN SPIN QUBITS WITH INDUCTORS

I began my research at the end of my freshman year. When my mentor first proposed a possible project, he was hesitant to point me in that direction because of its difficulty. Nevertheless, I eagerly accepted the challenge and spent several months stumbling on background information in quantum computing. This field attempts to use the quantum states of particles to process information. Physicists have engineered favorable quantum bits in semiconductors, but no quantum system has been able to outperform a classical computer. Experimentalists are interested in new ways to entangle quantum bits and we investigate alternative coupling methods for spin qubits that decrease their operation time. This project has expanded my interest in quantum mechanics and has taught me to think like a physicist by challenging my intuition and developing my ability to ask the right questions.

[LEFT] Physics Building, 2012. Photograph by Marlayna Demond, '11.

[RIGHT] Physics department, 1977, University Archives, Special Collections, University of Maryland, Baltimore County (UMBC).

INTRODUCTION

Universal computing can be dated to 1903 when Alan Turing's theoretical model of the Turing machine led a large-scale innovative revolution towards digital computing machines.[1] The next milestone is to process and control information at its fundamental level — quantum states of particles. Richard Feynman first pointed out that as certain types of computational problems get more complex, classical bits fail to give efficient answers.[2] For example, when simulating quantum mechanics, the amount of memory needed to describe a quantum system increases exponentially with the number of its components. A new device — a quantum computer — is therefore highly sought after by physicists.[3]

A quantum computer relies on the precise manipulation of quantum bits (qubits) to perform a two-qubit operation and hence generate an entangled state. Recent advances in solid-state physics have provided promising qubits by trapping electrons in artificial semiconductor quantum dots (Figure 1A).[4,5] For example, electrons trapped in a two-dimensional electron gas of GaAs-AlGaAs heterostructures can be encoded into singlet and triplet states and the two double quantum dots (DQDs) can entangle electrostatically (Figure 1B). While this system has reported coherence times of 200 ns, inter-qubit operations remain challenging because their non-local interactions are weak.[6]

SINGLET-TRIPLET QUBITS COUPLED TO RESONATOR VIA INDUCTOR

We propose a new quantum computing system that applies superconducting techniques to spin qubits. In theory, the entanglement of two capacitively coupled singlet-triplet qubits, which are particularly promising spin qubits, can be amplified with additional coupling through an inductive circuit element similar to the resonators used with superconducting qubits. Stronger coupling through the resonator yields faster operation times and hence a more viable quantum computer in a noisy spin environment.

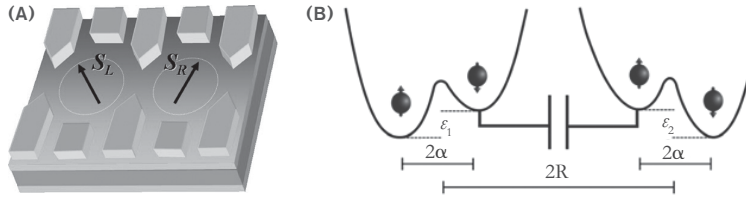

FIGURE 1. **(A)** Artificial double quantum dots confine electrons using lithographically etched nanowires. **(B)** Four electrons in two double quantum dots (DQDs). The spins of the two electrons in a DQD can form a singlet state $|S\rangle$ or triplet state $|T\rangle$. The Coulomb repulsion of each qubit (left and right DQD) provides non-local entangling terms in the Hamiltonian.

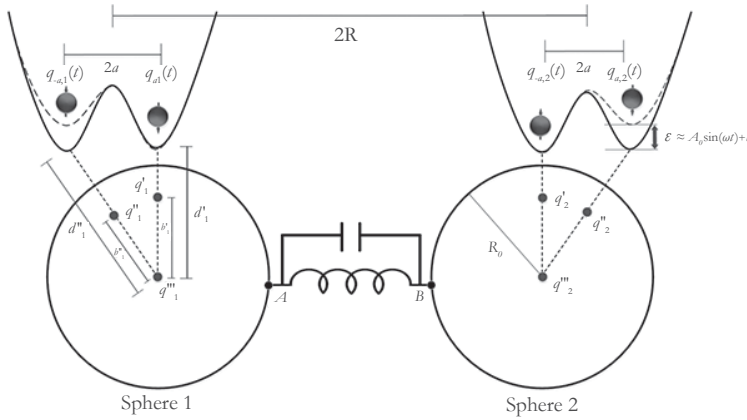

FIGURE 2. Method of images setup for induced charge on the end of the coupling element. Spheres were used to easily approximate the induced charge.

Previous theoretical models have proposed floating capacitive metallic gates that mediate the electrostatic interaction between the qubits.[7] Specifically, a pair of conducting discs connected by a wire placed near the DQDs allows the information of the qubits' states to propagate through the metal wire. The same idea is applicable to a coupler with a built-in inductor. The geometry of the metallic gate determines how the singlet-triplet qubits electrostatically interact with the coupler. To make the calculation manageable, we consider an inductive coupling element with conducting spheres attached to the ends (Figure 2). Because the electrons' probability densities are roughly Gaussian around the dot centers, they can be approximated as point charges. The number of electrons in the inner dots depends on the probability of the outer electrons tunneling inward when tilted with bias energy $\epsilon_{1,2}$ (Figure 1B). The charge configurations for the dots in Figure 2 are given by

$$q_{a,1}(t) = \langle \phi_a | e | \phi_a \rangle + \sin^2\theta(t) \langle \phi_{-a} | e | \phi_{-a} \rangle \quad (1.1)$$

$$q_{-a,1}(t) = \langle \phi_{-a} | e | \phi_{-a} \rangle - \sin^2\theta(t) \langle \phi_{-a} | e | \phi_{-a} \rangle \quad (1.2)$$

$$q_{-a,2}(t) = \langle \phi_{-a} | e | \phi_{-a} \rangle + \sin^2\theta(t) \langle \phi_a | e | \phi_a \rangle \quad (1.3)$$

$$q_{a,2}(t) = \langle \phi_a | e | \phi_a \rangle - \sin^2\theta(t) \langle \phi_a | e | \phi_a \rangle \quad (1.4)$$

where $\theta(t)$ is time-dependent when the dot is tilted sinusoidally because we choose $\epsilon(t) = A \sin \omega t + B$ (Appendix A). The voltage between the spheres is found by the method of images. For each charge, the boundary conditions for Laplace's equation can be satisfied by placing an image charge of magnitude $q'_{1/2} = \frac{R_0}{d'} q_{\pm a}$ at a distance $b = \frac{R_0^2}{d'}$ (Figure 2). Because the resonator is not grounded, each sphere has a floating potential V_0. Therefore a third image charge, $q'''(t)$, is placed at the center with magnitude $4\pi\epsilon R_0 V_0$. The potentials at nodes A and B are written as

$$V_A = \frac{q'''_1(t)}{4\pi\epsilon_0 R_0} = \frac{q(t) - q'_1(t) - q''_1(t)}{4\pi\epsilon_0 R_0} \quad (2.1)$$

$$V_B = \frac{q'''_2(t)}{4\pi\epsilon_0 R_0} = \frac{-q(t) - q'_2(t) - q''_2(t)}{4\pi\epsilon_0 R_0} \quad (2.2)$$

where $q(t)$ is the total induced charge on the sphere and, due to conservation of charge, is the opposite of the total induced charge on the other sphere ($q_{sphere1}(t) + q_{sphere2}(t) = 0$). The system is set up symmetrically with respect to the two qubits ($d_1 = d_2$), but each qubit is asymmetric ($d' \neq d''$). This way, the oscillating charge in the DQD induces an oscillating potential difference between the spheres. Depending on how the coupling element is engineered, it can be modeled as a parallel or series LC circuit coupled by a capacitor C_{eff} to a driving component $F(t)$. The qubits supply the driving potential $F(t) \sim (V_A - V_B)$ to the spheres. The total effective capacitance of the spherical ends of the resonator is $C_{eff} = 2\pi\epsilon_0 R_0 \approx 1.87$ aF and the AC driving potential $F(t) = (q_a'(t) - q_b'(t))/(4\pi\epsilon_0 R_0)$.

If the coupler is modeled as a series LC circuit, the effective capacitance of the spheres and the inherent capacitance of the coupler are added in series (Figure 3). The inherent capacitance of the coupler, C_2, can be modeled as a straight wire of radius 10 nm and length 1 μm. Because the capacitors are in series and $C_2 \sim fF \gg C_{eff}$, the inherent capacitance can be neglected (simplified circuit diagram in Figure 3).

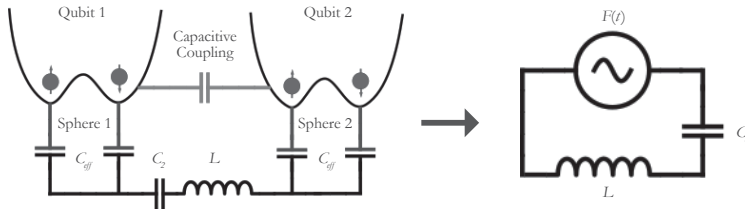

FIGURE 3. Circuit diagram of singlet-triplet qubits coupled to a series LC circuit. The capacitive coupling does not represent a physical capacitor — it is the Coulomb interaction of the two qubits. The qubits interact with the resonator through the effective capacitance of the spheres. The interaction can be simplified to the driven LC circuit on the right.

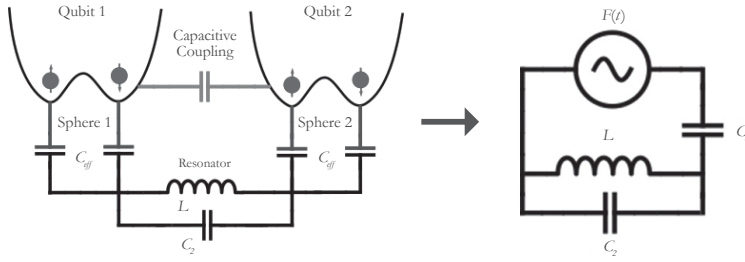

FIGURE 4. Circuit diagram of singlet-triplet qubits coupled to a parallel LC circuit.

Using Kirchhoff's voltage law, we set the potential difference between the spheres equal to the potential drop across the middle components of the coupler and ignore resistance: $V_{A\text{-}B} = V_L + V_{C_2} \approx V_L$.

$$F(t) - \frac{q(t)}{C_{eff}} - L\,\ddot{q}(t) = 0 \tag{3.1}$$

$$\ddot{q}(t) + \omega_0^2 q(t) = A' \sin \omega t + B' \tag{3.2}$$

where $\omega_0 = 1/\sqrt{LC}$. Appendix B gives A' and B' along with the solution for $q(t)$. If the coupling element is modeled as a parallel LC circuit (Figure 4), all of the drops in potential across branches are equal: $V_{A\text{-}B} = V_L = V_{C_2}$. Because of charge conservation, the three differential equations can be expressed as

$$F(t) - q_1(t) - L\,\ddot{q}_3(t) = 0 \tag{4.1}$$

$$F(t) - \frac{q_1(t)}{C_{eff}} - \frac{q_2(t)}{C_2} = 0 \tag{4.2}$$

$$\dot{q}_1(t) = \dot{q}_2(t) + \dot{q}_3(t) \tag{4.3}$$

where $q_1(t)$ is the charge on each sphere with effective capacitance C_{eff}, $q_2(t)$ is the charge on the capacitor C_2, and $q_3(t)$ is the current through each signal strip with inductance L. The resonant frequency of the system is $\omega_0 = \frac{1}{\sqrt{L(C_{eff} + C_2)}} \approx \frac{1}{\sqrt{LC_2}}$ (Appendix B).

Because the driving term is proportional to the charge difference between the spheres, the composite state where both qubits are in the singlet state, $|SS\rangle$, drives with $F(t) = 0$. $|TT\rangle$ is also static with sinusoidal tilting. Only the $|ST\rangle$ and $|TS\rangle$ states drive voltage across the coupler. The Hamiltonians of the series and parallel LC circuits are

$$H_{series} = [\frac{1}{8\pi\epsilon_0}\left(\frac{q(t)q_{\pm a}(t)}{d'} - \frac{q(t)}{d'}\right) + L\dot{q}(t)^2](I - \sigma_Z \otimes \sigma_Z) \quad (5.1)$$

$$H_{parallel} = [\frac{1}{8\pi\epsilon_0}\left(\frac{q_1(t)q_{\pm a\,1/2}(t)}{d'} - \frac{q_1(t)}{d'}\right) + \frac{q_2(t)}{2C_2} + L\dot{q}_3(t)^2](I - \sigma_Z \otimes \sigma_Z) \quad (5.2)$$

where $q(t)$ is the solution to Equation 3.2 and $q_1(t)$, $q_2(t)$, and $q_3(t)$ are all solutions to Equations 4.1–4.3 when $q_i(t = 0) = 0$ and $\dot{q}_i(t = 0) = 0$. The charge of the inner dot of a singlet-state qubit $q_{\pm a}(t)$ is periodic in time, while a triplet-state qubit contains static charge. We omit the interaction of the outer electrons because their charge terms can be absorbed into the terms of the inner electron.

ENTANGLEMENT DYNAMICS

The operation time of a two-qubit operation is the time it takes for the system to reach maximum entanglement. We quantify entanglement as the entropy in the system. It is calculated using the definition of von Neumann entropy:

$$S = -\sum_i \lambda_i \log_2 \lambda_i \quad (6)$$

where λ_i is the ith eigenvalue of the partial trace of the density matrix $\rho = \Sigma \rho_i |\psi_i\rangle\langle\psi_i|$. We numerically simulate Schrödinger's equation under different conditions using Equations 5.1 and 5.2.

We expect the peak entanglement time to be inversely proportional to the root mean square (RMS) of the $\sigma_z \otimes \sigma_z$ term in Equations 5.1 and 5.2. Amplifying this term should result in faster operation times. Because the solutions to Equation 3.2 and Equations 4.1–4.3 have amplitudes proportional to $1/(\omega^2 - \omega_0^2)$, the limit as ω approaches ω_0 yields $H_{RMS} \to \infty$ for the (2,2) and (3,3) elements. The beat period, $2\pi/(\omega_0 - \omega)$, approaches infinity as $\omega \to \omega_0$ because these solutions are superpositions of transient and steady-state components.

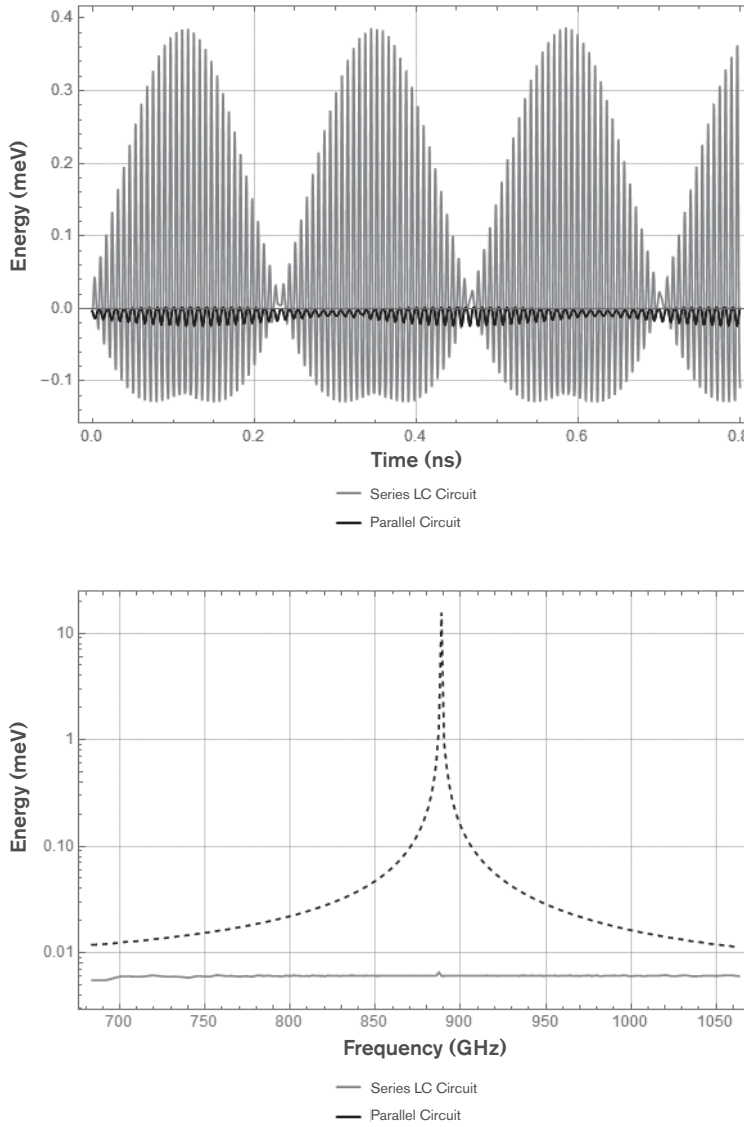

FIGURE 5. (A) The (2,2) Hamiltonian diagonal when driven within 3% away from resonance. For the series resonator, $\omega_0 \approx 888.6$ GHz and for the parallel resonator $\omega_0 \approx 628.4$ GHz. The qubits are driven with amplitude ≈ 0.25 meV. **(B)** RMS of the $\sigma_z \otimes \sigma_z$ components of the Hamiltonian. We expect τ_{ent} to be inversely proportional to the RMS. The parallel LC circuit has a peak within 1% away from ω_0, but it is small compared to that of the series circuit.

The envelope function, $\sin(\frac{\omega_0 - \omega}{2} t)$, carries the peak of the Hamiltonian towards infinity as resonance is approached. There is therefore a trade-off between amplifying the RMS of the Hamiltonian and taking time to ramp up the energy when driving the qubits.

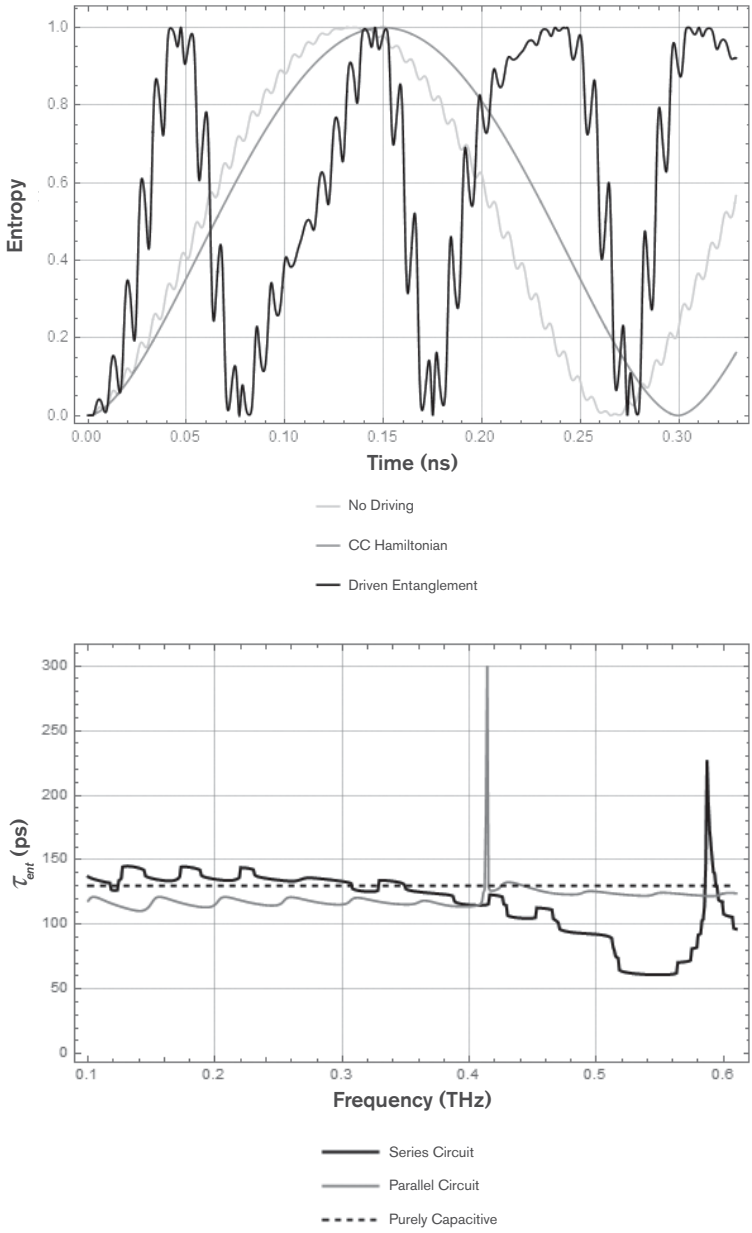

FIGURE 6. (A) Entanglement (von Neumann entropy) of qubits coupled to a series LC circuit. **(B)** Time to reach maximum entanglement time as a function of frequency. The optimal frequency is 6% away from resonance due to ramping effects of the driven oscillator.

We find that the dynamics of $H(t)$ are very sensitive to the choice of C_2. Previous experimental parameters have used C_2 = 100 fF, which is much larger than our aF values of C_{eff}.[8] It can be shown that $C_{eff} \ll C_2$ yields a rejecting circuit, which means that it has minimum current when driven at resonance. $C_{eff} \gg C_2$ also yields a rejecting circuit. We find that the RMS of the circuit, which responds to $\omega = 1\sqrt{2C_{eff}}$, is maximized when $C_{eff} = C_2$.

A comparison of the $|ST\rangle$ and $|TS\rangle$ diagonal elements of the series and parallel Hamiltonians (Equations 5.1 and 5.2) is plotted in Figure 5A. Each of these two components is influenced by the circuit, so each resembles a driven harmonic oscillator. The series LC circuit experiences more amplification than the parallel circuit does (Figure 5B). The parallel circuit also takes longer to ramp up in energy, making it a less ideal coupler for the qubits. The von Neumann entropy is plotted for the series LC resonator in Figure 6A. When the capacitively coupled qubits are tilted without the resonator, the nonlocal entanglement energy is $\alpha \approx 3$ meV, which corresponds to an operation time of $\tau_{ent} \approx 150$ ps. When the coupler is introduced to the system at a distance of 91 nm (roughly the height of the GaAs-AlGaAs structure previously used)[6] without driving, the electrostatic interaction of the qubits is slightly amplified such that the coefficient of the $\sigma_z \otimes \sigma_z$ component of $H_{circuit} \approx 9$ meV, so $\tau_{ent} \approx 130$ ps. We choose spheres that have $R_0 = a_B \approx 33.7$ nm, and the interqubit distance is $R = 7.5a_B$. We choose a value for inductance that was used in previous superconducting experiments: L ≈ 1.05 nH.[8]

For the series coupler, we find that τ_{ent} increases when the qubits are driven close enough to resonance (dark line in Figure 6B). This is because the ramping time of the resonator, and hence the interaction of qubits, is proportional to $1/(\omega - \omega_0)$. The optimal frequency is 834 GHz, which is 6.1% away from resonance, so the peak entanglement time is reduced to 40 ps (52% decrease). For the parallel circuit, we find that, for all frequencies, the long ramping time negates the advantages of the increased magnitude of the RMS of the Hamiltonian.

When engineering a resonating coupling element for spin qubits, it is best to avoid parallel capacitance. Although the parallel LC circuit offers a lower and more attainable resonant frequency, the requirement for C_2 to equal C_{eff} nullifies this advantage. Under current parameters, the series LC circuit improves the operation time of the singlet-triplet qubits by decreasing their entanglement time. The difficulty with this model is that C_{eff} dominates the resonance and causes the driving frequency to be too high, making it experimentally

inaccessible. To take advantage of the resonant speed-ups we have shown, one should instead inductively couple the qubits with a capacitance around 100 fF so that the resonance is in the GHz range.

CONCLUSION AND FUTURE WORK

Controlling systems at the quantum level has proven to be a challenging task that has motivated physicists to expand their experimental techniques. To perform a computation, a robust quantum computer must entangle multiple qubits before they decohere. The number of computations that a qubit system can execute is the ratio of the coherence time (≈320 ns for singlet-triplet qubits) to the operation time (≈140 ns).[6] Through simulations, the system we propose has been shown to improve operation time by over 50% by using an LC circuit amplifier to increase the coupling energy of the singlet-triplet qubits. Understanding the dynamics of oscillators and other amplification systems can expand the ideas and strategies that go into building a robust quantum computer.

APPENDIX A: CHARGE DISTRIBUTION DEPENDENCE ON AC DRIVE

Equations 1.1–1.4 describe the charge distribution among the four dots when tilted with bias energy ϵ. The interaction between two electrons in a single DQD is described by a 4 × 4 orbital Hamiltonian with basis $|S(2,0)\rangle$, $|S(0,2)\rangle$, $|S(1,1)\rangle$, $|T_0\rangle$:

$$H_{orb} = \begin{pmatrix} U+\epsilon & X & -\sqrt{t_0} & 0 \\ X & U-\epsilon & -\sqrt{t_0} & 0 \\ -\sqrt{t_0} & -\sqrt{t_0} & V_+ & 0 \\ 0 & 0 & 0 & V_- \end{pmatrix}$$

The tilt ϵ is set to zero when $U \gg \epsilon$, and U is the on-site Coulomb repulsion. Diagonalizing and isolating the matrix to only represent the

$$\tan\theta = \frac{2\sqrt{2}t_0}{U-\epsilon-V_+-\sqrt{(U-\epsilon-V_+)^2+8(t^0)^2}}$$

states of interest gives the tilting angle as a function of the bias energy: where t^0 is the tunneling amplitude between the two singlet states and V_+ is the Coulomb repulsion of the S(1,1) state. The bias energy is driven sinusoidally such that $\epsilon \approx A_0 \sin \omega t + b_0$, where A_0 is small and

b_0 is centered when $\sin\theta \approx \cos\theta$. The probability for the electron to tunnel as a function of time can be approximated using a first-order Taylor series:

$$\sin^2\theta = \frac{b_0 - U + V_+ + \sqrt{8(t_0^2) + (b_0 - U + V_+)^2}}{2\sqrt{8(t_0^2) + (b_0 - U + V_+)^2}} + \frac{4t_0^2 A_0 \sin\omega t}{(8t_0^2 + (B_0 - U + V_+)^2)^{3/2}}$$

Therefore the charge configurations in Equations 1.1–1.4 are sinusoidal, as is the forcing function in Equations 3.1, 4.1, and 4.2, because $F(t) = (q_a'(t) - q_b'(t))/(4\pi\epsilon_0 R_0)$.

APPENDIX B: SOLUTIONS TO KIRCHHOFF'S EQUATION

Equation 3.2 represents the dynamics of qubits coupled to a series circuit. Since $F(t)$ is sinusoidal, we can describe the nonhomogeneous driving term in the differential equation as $A'\sin\omega t + B'$ where

$$A' = \frac{4t_0^2 A(d' - d')}{4\pi\epsilon_0 d'd''(8t_0^2 + (b_0 - U + V_+)^2)^{3/2}}$$

$$B' = \frac{d' - d''}{8\pi\epsilon_0 d'd''}$$

In terms of A' and B', the solution to Equation 3.2 is

$$q(t) = \frac{B'\left(1 - \frac{\omega^2}{\omega_0^2}\right) - B'\left(1 - \frac{\omega^2}{\omega_0^2}\right)\cos\omega_0 t + A'\left(1 - \frac{\omega}{\omega_0}\right)\sin\omega t}{\Delta^2}$$

The differential equations in Equations 4.1–4.3 can be decoupled:

$$\ddot{q}_1(t) + \omega_0^2 = \frac{\ddot{F(t)}}{\frac{1}{C_{eff}} + \frac{1}{C_2}} + \frac{F(t)}{L\left(1 + \frac{C_2}{C_{eff}}\right)}$$

$$\ddot{q}_2(t) + \omega_0^2 q_2(t) = \frac{\ddot{F(t)}}{\frac{1}{C_{eff}} + \frac{1}{C_2}}$$

$$\ddot{q}_3(t) + \omega_0^2 q_3(t) = \frac{\ddot{F(t)}}{L\left(1 + \frac{C_2}{C_{eff}}\right)}$$

The solutions are found using *Mathematica* for $q_i(0) = 0$ and $\dot{q}_i(0) = 0$.

$$q_1(t) = \frac{B_1\Delta^2 - B_1\Delta^2\cos\omega t + A_1\omega_0(C_2L\omega^2 - 1)(\omega_0\sin\omega t) - \omega\sin\omega_0 t}{\Delta^2\omega_0^2 L\left(1 + \frac{C_2}{C_{eff}}\right)}$$

$$q_2(t) = \frac{A_1C_{eff}C_2\omega^2\sin\omega t}{\Delta^2(C_{eff} + C_2)} - \frac{A_1C_{eff}C_2\omega^3\sin\omega_0 t}{\Delta^2\omega_0(C_{eff} + C_2)}$$

$$i_3(t) = \frac{d}{dt}\left(\frac{A_1C_{eff}\omega^2\cos\omega t}{\Delta^2L(C_{eff} + C_2)} - \frac{A_1C_{eff}\omega^2\cos\omega t}{\Delta^2L(C_{eff} + C_2)}\right)$$

where

$$\Delta^2 = \omega^2 - \omega_0^2$$

$$A_1 = \frac{AC_{eff}t_0^2(C_2L\omega^2 - 1)}{(C_{eff} + C_2)d_1L\pi\epsilon_0(8t_0^2 + (-U + V_+ + b_0)^2)^{3/2}}$$

$$B_1 = -\frac{1}{L\left(\frac{C_2}{C_{eff}} + 1\right)4\pi\epsilon_0 d_1}$$

$$\omega_0 = \frac{1}{\sqrt{L(C_{eff} + C_2)}}$$

$$C_{eff} = 2\pi\epsilon_0 R_0$$

When driven at resonance, $\Delta^2 \rightarrow 0$, and all three solutions to Equation 4 diverge ($H_{RMS} \rightarrow \infty$).

REFERENCES

1. A. M. Turing, Proceedings of the London Mathematical Society s2-42, 230 (1937), http://plms.oxfordjournals.org/content/s2-42/1/230.full.pdf+html.
2. R. P. Feynman, International Journal of Theoretical Physics 21 (1982).
3. C. C. Mann, MIT Technology Review (2000).
4. D. Loss and D. P. DiVincenzo, Phys. Rev. A 57, 120(1998).
5. J. R. Petta, A. C. Johnson, A. Yacoby, C. M. Marcus, M. P. Hanson, and A. C. Gossard, Phys. Rev. B 72, 161301 (2005).
6. M. D. Shulman, O. E. Dial, S. P. Harvey, H. Bluhm, V. Umansky, and A. Yacoby, Science 336, 202 (2012), arXiv:1202.1828 [cond-mat.mes-hall].
7. L. Trifunovic, O. Dial, M. Trif, J. R. Wootton, R. Abebe, A. Yacoby, and D. Loss, Physical Review X 2, 1 (2012), arXiv:1110.1342.
8. M. Jerger, S. Poletto, P. Macha, U. Hbner, A. Lukashenko, E. Il'ichev, and A. V. Ustinov, EPL (Europhysics Letters) 96, 40112 (2011).